Appl. Phys. B 68, 325–332 (1999)

Applied Physics B
Lasers
and Optics

Third and fourth harmonic generation at Si-SiO_2 interfaces and in Si-SiO_2-Cr MOS structures

R.W. Kempf[1], P.T. Wilson[1], J.D. Canterbury[1], E.D. Mishina[2], O.A. Aktsipetrov[2], M.C. Downer[1]

[1] Department of Physics, The University of Texas at Austin, Austin, TX 78712, USA
[2] Department of Physics, Moscow State University, Moscow 119899, Russia

Received: 16 October 1998

Abstract. Third harmonic (TH) and fourth harmonic (FH) generation is systematically studied at unbiased buried Si(111)-SiO_2 and Si(110)-SiO_2 interfaces and DC-electric-field induced TH and FH generation is then observed in Si(111)-SiO_2-Cr and Si(110)-SiO_2-Cr MOS structures for the first time. A systematic phenomenological analysis of azimuthal anisotropy of TH and FH generation intensity is performed for (111) and (110) surfaces of O_h symmetric single crystals. A phenomenological model of electro-induced effects in TH and FH generation is then developed and the surface specificity and sensitivity of TH and FH generation are discussed. Optical interference of surface electro-induced and bulk bias-independent contributions to the effective third-order nonlinear polarization is proposed as the mechanism underlying surface sensitivity of electro-modulated TH probe.

PACS: 75.70.Ak; 75.70.Cn; 42.65

Surface and interface optics has been one of the most intensely studied fields in modern optics [1–3] for the last decade. Optical second harmonic generation (SHG) has comprised a major part of experimental and theoretical investigations in this field. Interest in SHG stems from its unique sensitivity to the structural and electronic properties of surfaces and interfaces of centrosymmetric media. This unusually high surface/interface-sensitivity comes about because the quadratic, and more generally all even-order, nonlinear susceptibilities vanish in the bulk of centrosymmetric materials [4, 5]. However, they are allowed at interfaces where inversion symmetry is broken by the discontinuity of the crystalline structure. Relevant nonlinear sources of even-order optical harmonics are often localized in a thin (several nanometers thick) surface or interface layer. Consequently SHG possesses extraordinary surface sensitivity compared to most optical probes.

Recently the next higher even-order nonlinear optical effect, fourth harmonic generation (FHG), has been observed in reflection from both noncentrosymmetric and centrosymmetric crystals [6]. Previously the weakness of the fourth-order surface nonlinear susceptibility $\chi^{(4)S}$ prevented its observation with fundamental light below the damage threshold. Sub-damage-threshold observation of FHG was enabled by state-of-the-art regeneratively amplified Ti:sapphire femtosecond laser systems. Further systematic studies of FHG and related effects may open up new nonlinear-optical probes which are more surface-specific and more sensitive to higher-order surface structure symmetries than SHG.

Another nonlinear optical probe of centrosymmetric materials, often neglected by researchers, is third harmonic generation (THG). THG is governed by a third order (more generally, odd-order) dipole susceptibility $\chi^{(3)B}$ which exists in the bulk of centrosymmetric media, and thus, generally speaking, is of limited usefulness as a diagnostic probe of interfaces. But in principle, THG and related phenomena can acquire some surface sensitivity through interference with surface-specific contributions modulated by external factors and because of the small escape depth of the THG radiation.

The influence of external factors on the SHG surface probe was demonstrated recently by electro-modulated SHG spectroscopy using Si-SiO_2-Cr MOS structures with a bias applied to a semitransparent metallic [7, 8] gate electrode. In centrosymmetric semiconductors, inversion symmetry is broken by the DC-electric field in the subsurface space charge region (SCR), which is created by initial band bending and/or application of an external bias. The lack of inversion symmetry in the SCR results in DC-electric-field induced second-harmonic (EFISH) generation, which manifests itself through electromodulation of the SHG intensity. Thus, important properties of surfaces, buried interfaces and subsurface layers – their charge [9], adsorption (adatom and admolecule surface density) [10, 11], initial band bending [12], etc. – can, in principle, be determined by means of the EFISH probe.

In this paper, THG and FHG are systematically studied at buried Si(111)-SiO_2 and Si(110)-SiO_2 interfaces, thus extending recent FHG studies at the Si(001)-SiO_2 interface [6]. Moreover, DC-electric field induced effects are observed, for the first time, to our knowledge, in third and fourth harmonic generation from Si-SiO_2-Cr MOS structures, also with (111) and (110) surface orientation. Anisotropic THG and FHG intensities and their bias dependences are studied.

DC-induced effects are suppressed by photoexcited carriers, which partially screen the static electric field in the semiconductor SCR [13]. Such photomodulation is especially strong for FHG, whose observation demands a large fundamental intensity. For this reason FH (and TH) studies were assisted by EFISH monitoring of the residual DC-electric field in the SCR to show that under a high level of optical excitation (to achieve a detectable FH signal) in silicon-based MOS this screening is incomplete and observation of DC-induced effects in FH generation is possible. The phenomenological model of DC-electric field induced effects developed in [14] for EFISH generation is extended to the description of electromodulation of higher harmonic intensity. Interference of surface DC-induced and bulk bias-independent contributions to the third-order nonlinear polarization is proposed as the mechanism underlying the observed surface sensitivity of DC-electric field induced TH generation.

1 Experimental

For SH, TH and FH generation the output of a regeneratively amplified Ti:sapphire laser system was used at a fundamental wavelength of 800 nm with a pulse energy of approximately 5 μJ, a repetition rate of 250 kHz and a pulse duration of 200 fs. The fundamental beam was focused on the sample surface at a 45° angle of incidence to a spot of about 50 μm diameter. The resulting fluence of $< 0.05\,\mathrm{J/cm^2}$ (which corresponds to peak intensity of $2.5 \times 10^{11}\,\mathrm{W/cm^2}$) is less than a half of the damage threshold [6]. Higher optical harmonic signals after dispersion in a Pellin–Broca prism were detected in three channels. TH or FH signals were additionally discriminated spectroscopically by appropriate bandpass filters and directed into a photon-counting system with background noise of less than 1 count/s. SHG used as a reference was detected simultaneously with the third or fourth harmonic by an analogous photon-counting system.

The anisotropic properties of higher optical harmonics are studied for n-Si highly doped (111) and (110) wafers covered by native oxide. The azimuthal anisotropy of FH, TH and SH intensity is studied by rotation of the samples with respect to the wafer surface normal.

Figure 1 shows the sets of azimuthal dependences of higher harmonic intensity measured for the Si(111) and Si(110) surfaces for various combinations of the fundamental and higher optical harmonic wave polarizations.

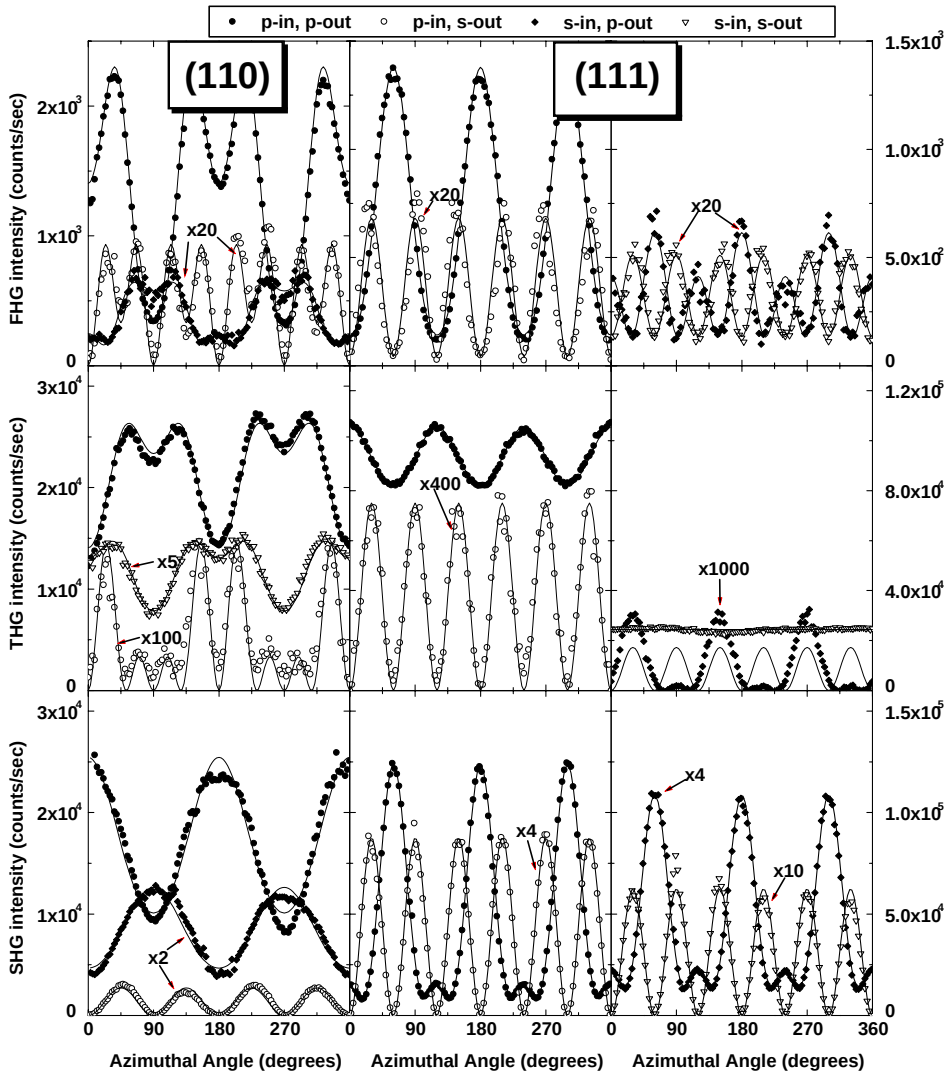

Fig. 1. Azimuthal dependences of the intensities of the harmonics for (110) (*left panel*) and (111) (*middle* and *right panels*) for various polarization combinations. *Solid lines*: fits to data using expressions for nonlinear polarization presented in Table 1. The fundamental wave intensity for SHG and THG is $I_\omega = 5 \times 10^9\,\mathrm{W/cm^2}$, and for FHG: $I_\omega = 2.5 \times 10^{11}\,\mathrm{W/cm^2}$. $\Psi = 0$ is along the $[1\bar{1}0]$ direction for Si(110) and the $[2\bar{1}\bar{1}]$ direction for Si(111)

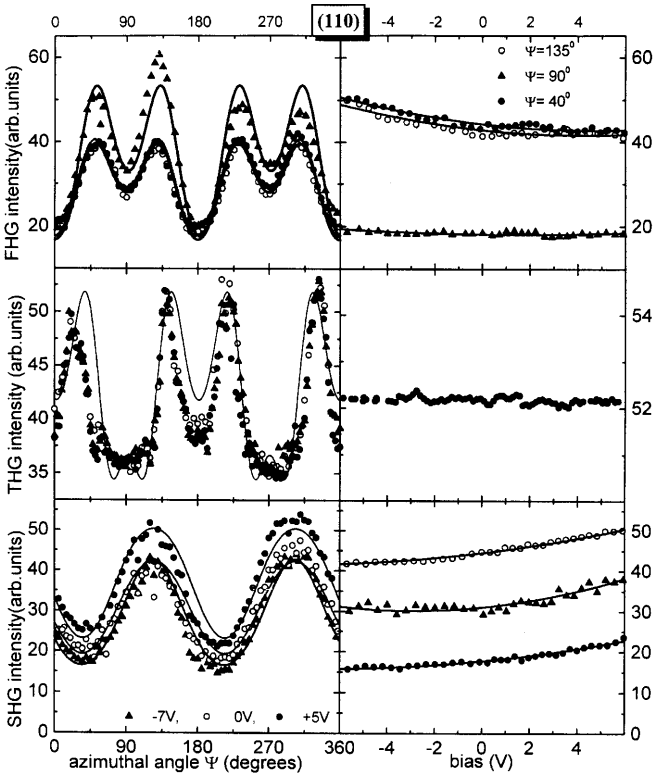

Fig. 2. *Left panels*: azimuthal dependences of FH intensity (*top panel*), TH intensity (*middle panel*) and SH intensity (*bottom panel*) measured for a Si(110)-SiO_2-Cr MOS structure at various biases. *Right panels*: bias dependences of corresponding *n*th harmonic intensity measured at the characteristic points of rotational anisotropy. Fundamental intensity for FHG is $I_\omega = 3.5 \times 10^{10}$ W/cm^2 (fluence $F = 7 \times 10^{-3}$ J/cm^2), for SHG and THG: $I_\omega = 10^9$ W/cm^2 (fluence $F = 7 \times 10^{-4}$ J/cm^2)

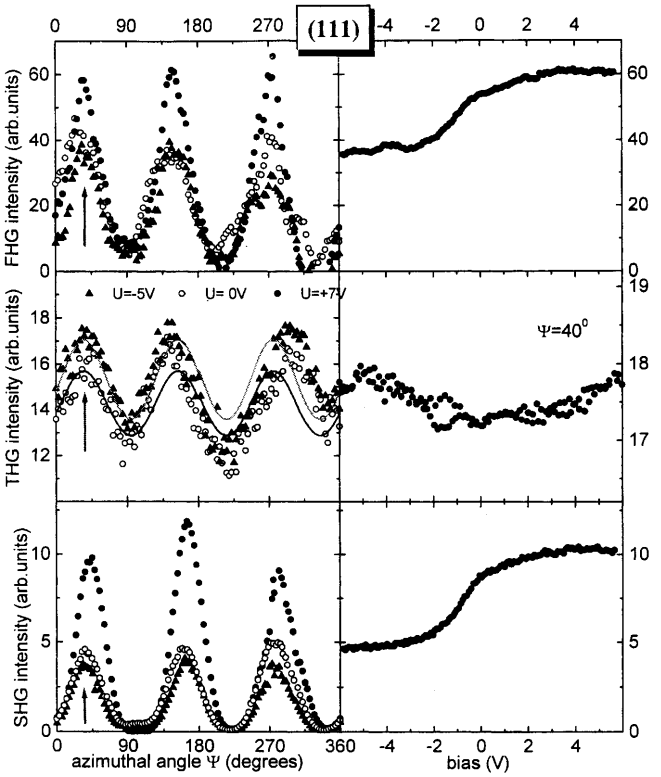

Fig. 3. *Left panels:* azimuthal dependences of FH intensity (*top panel*), TH intensity (*middle panel*) and SH intensity (*bottom panel*) measured for an Si(111)-SiO_2-Cr MOS structure at various biases. *Right panels:* bias dependences of correspondent *n*th harmonic intensity measured at the maximum of rotational anisotropy. Fundamental intensity for FHG is $I_\omega = 3.5 \times 10^{10}$ W/cm^2 (fluence $F = 7 \times 10^{-3}$ J/cm^2), for SHG and THG: $I_\omega = 10^9$ W/cm^2 (fluence $F = 7 \times 10^{-4}$ J/cm^2)

The MOS structures for studies of DC-induced effects were fabricated from highly doped n-Si (10^{17} cm^{-3} Sb doped) (111) and (110) wafers covered by a 24-nm thick SiO_2 film. A 3-nm thick semitransparent chromium cap electrode and an ohmic aluminum backside electrode were evaporated onto the samples. The external bias voltage was applied between the chromium and aluminum electrodes. SH, as well as TH and FH, signals from the chromium layer were verified to be negligible in comparison with signal from the Si-SiO_2 interface.

The bias dependences of the azimuthal anisotropy of SH, TH and FH intensity were studied. Figure 2 (left panel) shows the set of azimuthal dependences of the harmonic intensities measured for a Si(110)-SiO_2-Cr MOS structure at various biases. The left panels show the corresponding bias dependences of harmonic intensities measured at the maximum of rotational anisotropy. Figure 3 shows an analogous set of experimental data for a Si(111)-SiO_2-Cr MOS structure. The top panels in Figs. 2 and 3 show a pronounced bias dependence of FH intensity for both Si(110)-SiO_2 and Si(111)-SiO_2 interfaces. The middle panels in Figs. 2 and 3 show that DC-electric field effects in TH generation are very small at Si(111) and are not seen Si(110) MOS structures.

The bottom panels in Figs. 2 and 3 demonstrate EFISH generation which was recently studied in detail at Si(001)-SiO_2 interface. In our experiments EFISH generation serves as indicator of the presence of a DC-electric field in the SCR of silicon. Note that in contrast to SH and TH generation FH generation demands a much higher fundamental intensity. Thus, the observation of DC-induced FH requires a compromise. The fundamental intensity must be high enough to generate a detectable FH signal, but photoexcited carriers must not completely screen the DC-electric field in the SCR. Figure 4 shows the EFISH bias dependence measured at various fluences of fundamental radiation. The role of the photoexcited free carriers is clear from comparison of EFISH bias de-

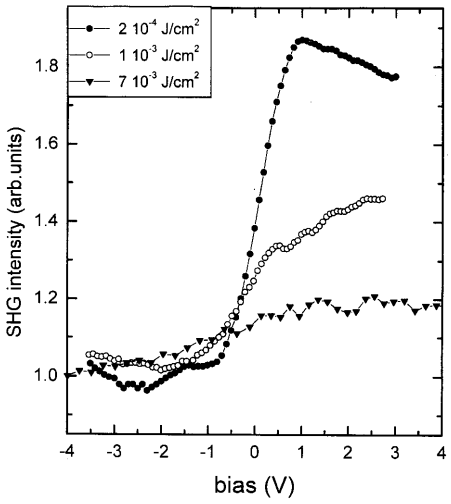

Fig. 4. EFISH dependences measured at various fluences of fundamental radiation

pendence at $F = 2 \times 10^{-4}\,\mathrm{J/cm^2}$ and $F = 7 \times 10^{-3}\,\mathrm{J/cm^2}$ in Fig. 4. Larger fluences suppress the bias dependence through screening of the interface field. However, the SH intensity measured at a fundamental fluence of $F = 7 \times 10^{-3}\,\mathrm{J/cm^2}$ shows a noticeable bias dependence which indicates the existence of a residual DC-electric field in the semiconductor SCR despite significant photoexcited carrier screening. On the other hand, a fluence of $F = 7 \times 10^{-3}\,\mathrm{J/cm^2}$ allows the detection of FH generation without fully screening the interface field.

2 Discussion

Two main sources of approximately the same order of magnitude, surface dipole and bulk quadrupole, contribute to the even-order nonlinear polarization $P(n\omega)$ of the Si/SiO_2 interface which is given by

(i) for SH:

$$P_i(2\omega) = \chi_{ijkl}^{(2)\,\mathrm{bulk,\,Q}} E_j^{\omega} E_k^{\omega} E_l^{\omega} + \chi_{ijk}^{(2)\,\mathrm{surf,\,D}} E_j^{\omega} E_k^{\omega} , \qquad (1)$$

where $\chi_{ijkl}^{(2)\,\mathrm{bulk,\,Q}}$ is the second-order bulk quadrupole susceptibility, $\chi_{ijk}^{(2)\,\mathrm{surf,\,D}}$ is the second-order surface dipole susceptibility, E_j^{ω} is the amplitude j-component of the fundamental wave, and E_k^{ω} is the k-component of the fundamental wavevector;

(ii) for FH:

$$P_i(4\omega) = \chi_{ijklm}^{(4)\,\mathrm{surf,\,D}} E_j^{\omega} E_k^{\omega} E_l^{\omega} E_m^{\omega} + \chi_{ijklmn}^{(4)\,\mathrm{bulk,\,Q}} E_j^{\omega} E_k^{\omega} E_l^{\omega} E_m^{\omega} E_n^{\omega} , \qquad (2)$$

where $\chi_{ijklm}^{(4)\,\mathrm{surf,\,D}}$ and $\chi_{ijklmn}^{(4)\,\mathrm{bulk,\,Q}}$ are the fourth-order surface dipole and bulk quadrupole susceptibilities, respectively.

For the odd-order optical harmonics the main dipole contribution comes from the bulk, therefore, the third-order polarization is given by:

(iii) for TH:

$$P_i(3\omega) = \chi_{ijkl}^{(3)\,\mathrm{bulk,\,D}} E_j^{\omega} E_k^{\omega} E_l^{\omega} , \qquad (3)$$

where $\chi_{ijkl}^{(3)\,\mathrm{bulk,\,D}}$ is the third-order bulk dipole susceptibility.

Various nonlinear sources in the semiconductor corresponding to the various terms in (1)–(3) possess different (surface or bulk) location, so propagation functions are different for harmonic waves excited by these different sources. Analytically this can be taken into account by a convolution of the nonlinear polarization with the appropriate Green function. The amplitude of electric field of the nth harmonic wave is given by

(i) for the bulk dipole terms:

$$E^{\mathrm{bulk,\,D}}(n\omega) = \int_0^{\infty} P^{\mathrm{bulk,\,D}}(n\omega) G_n^{\mathrm{BD}}(z')\,\mathrm{d}z' \qquad (4)$$

$$\cong \boldsymbol{p} F_{n\omega} F_{\omega}^{n} \chi^{(n),\,\mathrm{bulk,\,D}} \frac{\mathrm{i}}{n k_{z,\omega} + k_{z,n\omega}} (E^{\omega})^n ,$$

where $G_n^{\mathrm{BD}}(z')$ is the Green function for the nonlinear wave equation with the appropriate boundary conditions, F_{ω} is the Fresnel factor at the fundamental wavelength, $F_{n\omega}$ is the Fresnel factor at the nth harmonic wavelength, l_n^{eff} is the effective thickness of the silicon subsurface layer that contributes to the nth harmonic intensity, $\boldsymbol{p}$ is the unit polarization vector and $k_{z,n\omega}$ is the z-component of the nth harmonic wavevector;

(ii) for the bulk quadrupole terms:

$$E^{\mathrm{bulk,\,Q}}(n\omega) = \int_0^{\infty} P^{\mathrm{bulk,\,Q}}(n\omega) G_n^{\mathrm{BQ}}(z')\,\mathrm{d}z' \qquad (5)$$

$$\cong \boldsymbol{p} F_{n\omega} F_{\omega}^{n} \chi^{(n),\,\mathrm{bulk,\,Q}} \frac{k_{z,\omega}}{n k_{z,\omega} + k_{z,n\omega}} (E^{\omega})^n ,$$

(iii) for the surface dipole term:

$$E^{\mathrm{surf,\,D}}(n\omega) = \int_0^{\infty} P^{\mathrm{SD}}(n\omega) G(z') \delta(z')\,\mathrm{d}z = \boldsymbol{p} F_{n\omega} F_{\omega}^{n} \chi_{\mathrm{surf}}^{(n)} (E^{\omega})^n , \qquad (6)$$

where the effective surface susceptibility $\chi_{\mathrm{surf}}^{(n)}$ is determined following [15].

Integration in (4)–(6) formally should be done over semi-infinite bulk of the semiconductor; however, in a reflection geometry the main part of the integral comes from the area that is restricted by effective thickness l_n^{eff}. Figure 5 shows the propagation functions for the nth harmonic waves. For the fundamental wavelength used in our experiments the effective thickness for SH radiation is determined mostly by the real part of the wavevectors $\boldsymbol{k}_{\omega}$ and $\boldsymbol{k}_{2\omega}$: $l_2^{\mathrm{eff}} \cong \lambda_{\omega}/2(n(\omega) + n(2\omega)) = 40\,\mathrm{nm}$, where $n(\omega)$, $n(2\omega)$ are the refractive indices at the fundamental and SH wavelengths. This effective thickness is analogous to the coherence length in the case of transmission geometry. For TH and FH generation the effective thickness is determined mostly by the imaginary part of the wavevectors $\boldsymbol{k}_{3\omega}$ and $\boldsymbol{k}_{4\omega}$:

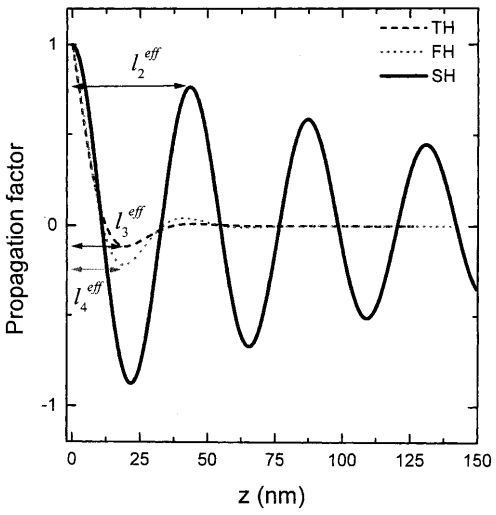

Fig. 5. Propagation functions for SH, TH and FH waves in silicon at 800 nm fundamental wavelength

$l_n^{\text{eff}} \cong 1/k_{z,n_\omega} = \lambda_{n_\omega}/2\pi\kappa(n\omega)$ (where $\kappa(n\omega)$ is the imaginary part of the refractive index at the nth harmonic wavelength). This effective thickness is the escape depth of the corresponding electromagnetic wave and is approximately 10 nm for both TH and FH.

It was shown in [6] that for the GaAs(001) surface the separation of surface and bulk contributions to SH and FH generation is possible due to the different rotational azimuthal symmetry of these contributions. However, due to the higher symmetry of silicon, the only excluded contribution is the bulk quadrupole term for SH from the (110) (see Table 1). Solid lines in Fig. 1 show the fit to the experimental azimuthal dependences of the equations in Table 1. The amplitudes of all Fourier components obtained from these data are shown in Table 2. The perfect fit of the experimental data for FHG proves that the much higher fundamental intensity necessary for FHG observation in comparison with fundamental intensity in SHG and THG experiments does not influence the structure of the subsurface layer, allowing a true probing of the higher-order symmetry of the solid surface.

In the presence of a strong DC-electric-field at the Si/SiO_2 interface additional DC-induced contributions appear in the expression for nonlinear polarizations. For even-order harmonics they originate from the space charge region and are described in the dipole approximation by the odd-order nonlinear susceptibility

(i) for SH:

$$P_i(2\omega, E_{0z}) = \chi_{ijkz}^{(3)\,\text{bulk, D}} E_j^\omega E_k^\omega E_{0z}(z)\,, \tag{7}$$

where $\chi_{ijkz}^{(3)\,\text{bulk, D}}$ is the third-order bulk dipole susceptibility, $E_{0z}(z)$ is the strength of the DC-electric field;

(ii) for FH:

$$P_i(4\omega, E_{0z}) = \chi_{ijklmz}^{(5)\,\text{bulk, D}} E_j^\omega E_k^\omega E_l^\omega E_m^\omega E_{0z}(z)\,, \tag{8}$$

where $\chi_{ijklmz}^{(5)\,\text{bulk, D}}$ is the fifth-order bulk dipole susceptibility. The bulk dipole character of these terms make them of the same order of magnitude as the bulk quadrupole and surface dipole terms.

For SH and FH generation, the main dipole bias-dependent contribution comes from the bulk. The bulk third-order dipole DC-induced polarization equals zero as it is described by the fourth-order nonlinear susceptibility, which vanishes in a centrosymmetric media. Therefore, no DC-electric-field TH is expected from the bulk in the dipole approximation. The next third-order nonlinear polarization in the centrosymmetric material is the surface DC-induced contribution which is given by

(iii) for TH:

$$P_i(3\omega) = \chi_{ijklz}^{(4)\,\text{surf, D}} E_j^\omega E_k^\omega E_l^\omega E_{0z}(z)\,. \tag{9}$$

Table 1. Azimuthal dependence of polarizations at the FH, TH and SH wavelengths excited by surface dipole, bulk dipole and bulk quadrupole (field-independent) nonlinear sources

		(111)	(110)
FHG	p-p	$P_{4,pp}^{\text{BQ}} = a_{4,pp}^{\text{BQ}} + b_{4,pp}^{\text{BQ}}\cos(3\Psi) + c_{4,pp}^{\text{BQ}}\cos(6\Psi)$	$P_{4,pp}^{\text{BQ}} = a_{4,pp}^{\text{BQ}} + b_{4,pp}^{\text{BQ}}\cos(2\Psi) + c_{4,pp}^{\text{BQ}}\cos(4\Psi) + d_{4,pp}^{\text{BQ}}\cos(6\Psi)$
		$P_{4,pp}^{\text{SD}} = a_{4,pp}^{\text{SD}} + b_{4,pp}^{\text{SD}}\cos(3\Psi)$	$P_{4,pp}^{\text{SD}} = a_{4,pp}^{\text{SD}} + b_{4,pp}^{\text{SD}}\cos(2\Psi) + c_{4,pp}^{\text{SD}}\cos(4\Psi)$
	p-s	$P_{4,ps}^{\text{BQ}} = b_{4,ps}^{\text{BQ}}\sin(3\Psi) + c_{4,ps}^{\text{BQ}}\sin(6\Psi)$	$P_{4,ps}^{\text{BQ}} = b_{4,ps}^{\text{BQ}}\sin(2\Psi) + c_{4,ps}^{\text{BQ}}\sin(4\Psi) + d_{4,ps}^{\text{BQ}}\sin(6\Psi)$
		$P_{4,ps}^{\text{SD}} = b_{4,ps}^{\text{SD}}\sin(3\Psi)$	$P_{4,ps}^{\text{SD}} = b_{4,ps}^{\text{SD}}\sin(2\Psi) + c_{4,ps}^{\text{SD}}\sin(4\Psi)$
	s-p	$P_{4,sp}^{\text{BQ}} = a_{4,ps}^{\text{BQ}} + b_{4,sp}^{\text{BQ}}\cos(3\Psi) + c_{4,sp}^{\text{BQ}}\cos(6\Psi)$	$P_{4,sp}^{\text{BQ}} = a_{4,ps}^{\text{BQ}} + b_{4,sp}^{\text{BQ}}\cos(2\Psi) + c_{4,sp}^{\text{BQ}}\cos(4\Psi) + d_{4,sp}^{\text{BQ}}\cos(6\Psi)$
		$P_{4,sp}^{\text{SD}} = a_{4,sp}^{\text{SD}} + b_{4,sp}^{\text{SD}}\cos(3\Psi)$	$P_{4,sp}^{\text{SD}} = a_{4,sp}^{\text{SD}} + b_{4,sp}^{\text{SD}}\cos(2\Psi) + c_{4,sp}^{\text{SD}}\cos(4\Psi)$
	s-s	$P_{4,ss}^{\text{BQ}} = b_{4,ss}^{\text{BQ}}\sin(3\Psi) + c_{4,ss}^{\text{BQ}}\sin(6\Psi)$	$P_{4,ss}^{\text{BQ}} = b_{4,ss}^{\text{BQ}}\sin(2\Psi) + c_{4,ss}^{\text{BQ}}\sin(4\Psi) + d_{4,ss}^{\text{BQ}}\sin(6\Psi)$
		$P_{4,ss}^{\text{SD}} = b_{4,ss}^{\text{SD}}\sin(3\Psi)$	
THG	p-p	$P_{3,pp}^{\text{BD}} = a_{3,pp}^{\text{BD}} + b_{3,pp}^{\text{BD}}\cos(3\Psi)$	$P_{3,pp}^{\text{BD}} = a_{3,pp}^{\text{BD}} + b_{3,pp}^{\text{BD}}\cos(2\Psi) + c_{3,pp}^{\text{BD}}\cos(4\Psi)$
	p-s	$P_{3,ps}^{\text{BD}} = b_{3,ps}^{\text{BD}}\sin(3\Psi)$	$P_{3,ps}^{\text{BD}} = b_{3,ps}^{\text{BD}}\sin(2\Psi) + c_{3,ps}^{\text{BD}}\sin(4\Psi)$
	s-p	$P_{3,sp}^{\text{BD}} = b_{3,sp}^{\text{BD}}\sin(3\Psi)$	$P_{3,sp}^{\text{BD}} = b_{3,sp}^{\text{BD}}\sin(2\Psi) + c_{3,sp}^{\text{BD}}\sin(4\Psi)$
	s-s	$P_{3,sp}^{\text{BD}} = a_{3,sp}^{\text{BD}}$	$P_{3,ss}^{\text{BD}} = a_{3,ss}^{\text{BD}} + b_{3,ss}^{\text{BD}}\cos(2\Psi) + c_{3,ss}^{\text{BD}}\cos(4\Psi)$
SHG	p-p	$P_{2,pp}^{\text{BQ}} = a_{2,pp}^{\text{BQ}} + b_{2,pp}^{\text{BQ}}\cos(3\Psi)$	$P_{2,pp}^{\text{BQ}} = a_{2,pp}^{\text{BQ}} + b_{2,pp}^{\text{BQ}}\cos(2\Psi) + c_{2,pp}^{\text{BQ}}\cos(4\Psi)$
		$P_2^{\text{SD}} = a_{2,pp}^{\text{SD}} + b_{2,pp}^{\text{SD}}\cos(3\Psi)$	$P_2^{\text{SD}} = a_{2,pp}^{\text{SD}} + b_{2,pp}^{\text{SD}}\cos(2\Psi)$
	p-s	$P_{2,ps}^{\text{BQ}} = b_{2,ps}^{\text{BQ}}\sin(3\Psi)$	$P_{2,ps}^{\text{BQ}} = b_{2,ps}^{\text{BQ}}\sin(2\Psi) + c_{2,ps}^{\text{BQ}}\sin(4\Psi)$
		$P_{2,pp}^{\text{SD}} = b_{2,ps}^{\text{SD}}\sin(3\Psi)$	$P_{2,ps}^{\text{SD}} = b_{2,ps}^{\text{SD}}\sin(2\Psi)$
	s-p	$P_{2,sp}^{\text{BQ}} = a_{2,sp}^{\text{BQ}} + b_{2,sp}^{\text{BQ}}\cos(3\Psi)$	$P_{2,sp}^{\text{BQ}} = a_{2,sp}^{\text{BQ}} + b_{2,sp}^{\text{BQ}}\cos(2\Psi) + c_{2,sp}^{\text{BQ}}\cos(4\Psi)$
		$P_{2,sp}^{\text{SD}} = a_{2,sp}^{\text{SD}} + b_{2,sp}^{\text{SD}}\cos(3\Psi)$	$P_{2,sp}^{\text{SD}} = a_{2,sp}^{\text{SD}} + b_{2,sp}^{\text{SD}}\cos(2\Psi)$
	s-s	$P_{2,ss}^{\text{BQ}} = b_{2,ss}^{\text{BQ}}\sin(3\Psi)$	$P_{2,ss}^{\text{BQ}} = b_{2,ss}^{\text{BQ}}\sin(2\Psi) + c_{2,ss}^{\text{BQ}}\sin(4\Psi)$
		$P_{2,ss}^{\text{SD}} = b_{2,ss}^{\text{SD}}\sin(3\Psi)$	

Table 2. Fourier amplitudes of FH, TH and SH polarization excited by surface dipole, bulk dipole and bulk quadrupole nonlinear sources

		(111)	(110)
FHG		$a^{\mathrm{BQ}}_{4,pp}+a^{\mathrm{SD}}_{4,pp}=24\pm1\mathrm{e}^{-1.9\pm1\,\mathrm{i}}$, $b^{\mathrm{BQ}}_{4,pp}+b^{\mathrm{SD}}_{4,pp}=14\pm1\,\mathrm{e}^{1\pm1\,\mathrm{i}}$, $c^{\mathrm{BQ}}_{4,pp}=9\pm3$	$a^{\mathrm{BQ}}_{4,pp}+a^{\mathrm{SD}}_{4,pp}=35.4\pm0.6\mathrm{e}^{-0.3\pm0.1\,\mathrm{i}}$, $b^{\mathrm{BQ}}_{4,pp}+b^{\mathrm{SD}}_{4,pp}=16\pm1\mathrm{e}^{2.7\pm0.1\,\mathrm{i}}$, $c^{\mathrm{BQ}}_{4,pp}+c^{\mathrm{SD}}_{4,pp}=11\pm1$
	p-s	$b^{\mathrm{BQ}}_{4,ps}+b^{\mathrm{SD}}_{4,ps}=5.7\pm0.5\,\mathrm{e}^{0\,\mathrm{i}}$, $c^{\mathrm{BQ}}_{4,pp}=0.7\pm0.3$	$b^{\mathrm{BQ}}_{4,ps}+b^{\mathrm{SD}}_{4,ps}=4.1\pm0.8\,\mathrm{e}^{1.6\pm0.1\,\mathrm{i}}$, $c^{\mathrm{BQ}}_{4,pp}+c^{\mathrm{SD}}_{4,pp}=6.2\pm0.6$
	s-p	$a^{\mathrm{BQ}}_{4,sp}+a^{\mathrm{SD}}_{4,sp}=3.1\pm0.1\mathrm{e}^{0.85\pm0.09\,\mathrm{i}}$, $b^{\mathrm{BQ}}_{4,sp}+b^{\mathrm{SD}}_{4,sp}=3.5\,\mathrm{e}^{2.5\pm0.3\,\mathrm{i}}$, $c^{\mathrm{BQ}}_{4,sp}=0.8\pm0.3$	$a^{\mathrm{BQ}}_{4,sp}+a^{\mathrm{SD}}_{4,sp}=4.4\pm0.1\,\mathrm{e}^{-0.5\pm0.5\,\mathrm{i}}$, $b^{\mathrm{BQ}}_{4,sp}+b^{\mathrm{SD}}_{4,sp}=1.8\pm0.3\,\mathrm{e}^{3.3\pm0.5\,\mathrm{i}}$, $c^{\mathrm{BQ}}_{4,sp}+c^{\mathrm{SD}}_{4,sp}=0.4\pm0.4\,\mathrm{e}^{1.5\pm0.5\,\mathrm{i}}$, $d^{\mathrm{BQ}}_{4,sp}=0.6\pm0.4$
	s-s	$b^{\mathrm{BQ}}_{4,ps}+b^{\mathrm{SD}}_{4,ps}=4.4\pm0.2\,\mathrm{e}^{2.4\pm0.3\,\mathrm{i}}$, $c^{\mathrm{BQ}}_{4,pp}=0.6\pm0.3$	0
THG	p-p	$a^{\mathrm{BQ}}_{3,pp}=305\pm3\,\mathrm{e}^{0.7\pm0.3\,\mathrm{i}}$, $b^{\mathrm{BQ}}_{3,pp}=25\pm12$	$a^{\mathrm{BD}}_{3,pp}=147\pm3\,\mathrm{e}^{3.4\pm0.1\,\mathrm{i}}$, $b^{\mathrm{BD}}_{3,pp}=24\pm4\,\mathrm{e}^{-0.5\pm0.3\,\mathrm{i}}$, $c^{\mathrm{BD}}_{3,pp}=12\pm3$
	p-s	$b^{\mathrm{BQ}}_{3,ps}=13.7\pm0.5$	$b^{\mathrm{BD}}_{3,ps}=4.4\pm0.3\,\mathrm{e}^{0\pm0.7\,\mathrm{i}}$, $c^{\mathrm{BD}}_{3,ps}=8.8\pm0.4$
	s-p	$b^{\mathrm{BQ}}_{3,sp}=4\pm4$	$b^{\mathrm{BD}}_{3,sp}=5\pm3\,\mathrm{e}^{3\pm6\,\mathrm{i}}$, $c^{\mathrm{BD}}_{3,sp}=7\pm2$
	s-s	$a^{\mathrm{BQ}}_{3,sp}=150\pm20$	$a^{\mathrm{BD}}_{3,ss}=49\pm1\,\mathrm{e}^{2.8\pm0.1\,\mathrm{i}}$, $b^{\mathrm{BD}}_{3,ss}=9\pm2\,\mathrm{e}^{3.7\pm0.2\,\mathrm{i}}$, $c^{\mathrm{BD}}_{3,pp}=4\pm1$
SHG	p-p	$a^{\mathrm{BQ}}_{2,pp}+a^{\mathrm{SD}}_{2,pp}=162\pm5\,\mathrm{e}^{2.51\pm0.03\,\mathrm{i}}$, $b^{\mathrm{BQ}}_{2,pp}+b^{\mathrm{SD}}_{2,pp}=208\pm6$	$a^{\mathrm{BQ}}_{2,pp}+a^{\mathrm{SD}}_{2,pp}=129\pm2\,\mathrm{e}^{2.5\pm1\,\mathrm{i}}$, $b^{\mathrm{BQ}}_{2,pp}+b^{\mathrm{SD}}_{2,pp}=36\pm4\,\mathrm{e}^{1.9\pm0.9\,\mathrm{i}}$, $c^{\mathrm{BQ}}_{2,pp}=7\pm3$
	p-s	$b^{\mathrm{BQ}}_{2,ps}+b^{\mathrm{SD}}_{2,ps}=148\pm3$	$b^{\mathrm{BQ}}_{2,ps}+b^{\mathrm{SD}}_{2,ps}=37\pm2\,\mathrm{e}^{-1\pm6\,\mathrm{i}}$, $c^{\mathrm{BQ}}_{2,ps}=3\pm9$
	s-p	$a^{\mathrm{BQ}}_{2,sp}+a^{\mathrm{SD}}_{2,sp}=81\pm4\,\mathrm{e}^{2.32\pm0.05\,\mathrm{i}}$, $b^{\mathrm{BQ}}_{2,sp}+b^{\mathrm{SD}}_{2,sp}=98\pm4$	$a^{\mathrm{BQ}}_{2,sp}+a^{\mathrm{SD}}_{2,sp}=63\pm3\,\mathrm{e}^{3.6\pm0.9\,\mathrm{i}}$, $b^{\mathrm{BQ}}_{2,sp}+b^{\mathrm{SD}}_{2,sp}=17\pm3\,\mathrm{e}^{0.2\pm0.6\,\mathrm{i}}$, $c^{\mathrm{BQ}}_{2,sp}=3\pm2$
	s-s	$b^{\mathrm{BQ}}_{2,ss}+b^{\mathrm{SD}}_{2,ss}=79\pm4$	0

The amplitude of the electric field of the DC-induced SH or FH wave at the detector can be written as:

$$E^{\mathrm{bulk,\,D}}(n\omega,E_0)=\int_0^{\infty}P^{\mathrm{bulk,\,D}}\left(n\omega,E_0(z')\right)G_n^{\mathrm{BD}}(z')\,\mathrm{d}z'$$
$$\cong pF_{n\omega}F_{\omega}^{n}\chi^{(n+1)}\,(E^{\omega})^{n}\times\int_0^{l_n^{\mathrm{eff},E_0}}E_0(z')\mathrm{e}^{-\mathrm{i}(nk_{z,\omega}+k_{z,n\omega})z'}\,\mathrm{d}z'\,,\qquad(10)$$

where l_n^{eff,E_0} is the effective thickness of the silicon subsurface layer for DC-induced nth harmonic generation.

To obtain the DC-electric field spatial distribution the Poisson equation with the appropriate boundary conditions must be solved [14]. Numerical calculations of the Poisson equation give the spatial behavior of the integrand of (10). Figure 6 shows the results of such numerical calculations for DC-induced SH, FH waves for several values of the surface potential, determined as $\varphi_{\mathrm{S}}=-\int_0^{\infty}E_0(z')\,\mathrm{d}z'$. These results show that at 800 nm the thickness of the subsurface layers contributing to DC-induced nth harmonic signal is 40 nm for SH and 10 nm for FH.

If the DC-induced harmonic wave is predominant, the dependence of the harmonic intensity should be parabolic with the minimum at a zero surface potential. Two factors influence the shape of the experimental dependence of the higher harmonic intensities on the applied bias. The first factor is connected with electrophysical property of the interface. The DC-field in the semiconductor satisfies the boundary conditions, taking into account a bias drop across semiconductor and at the interface states: $U=\varepsilon_{\mathrm{Si}}\varepsilon_{\mathrm{ox}}^{-1}E_0(\varphi_{\mathrm{S}})L_{\mathrm{ox}}+\varphi_{\mathrm{S}}$, where $\varepsilon_{\mathrm{Si}}$, $\varepsilon_{\mathrm{ox}}$ are the permittivity of the silicon and silicon oxide, respectively; $E_0(\varphi_{\mathrm{S}})$ is the surface DC-electric field and L_{ox} is the thickness of the oxide layer. This yields a complicated bias dependence of the surface potential. In turn, this leads to the deviation of bias dependences of higher harmonic intensities from parabolic while the voltage of the minimum of these bias dependences remains at the zero value of the surface potential, the flat band voltage. The second factor changing the shape of the experimental bias dependence of

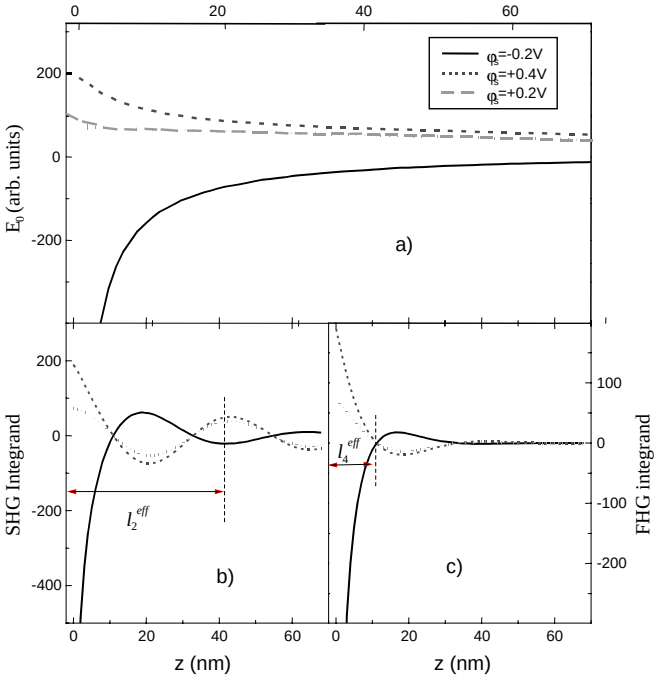

Fig. 6. a Spatial distribution of DC-electric-field for Si/SiO_2 MOS structure (n-type, $N_D = 10^{17}\,cm^{-3}$) for various surface potentials; **b**, **c** spatial distribution of integrand in (10) for **b** SH, and **c** FH

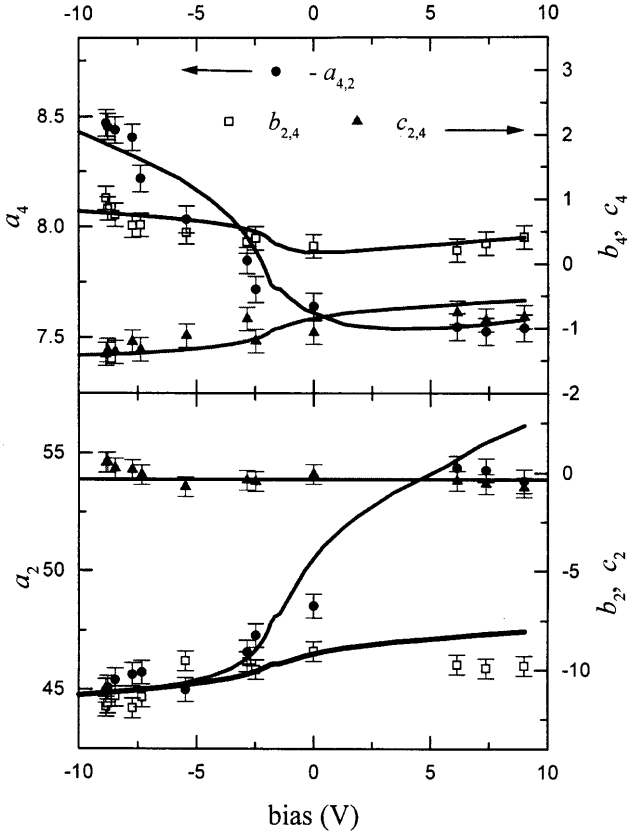

Fig. 7. Bias dependences of Fourier components $a_n = a_n^{BD} + a_n^{SD} + a_n^{BD}(E_0)$ (*left-hand scale*), $b_n = b_n^{BD} + b_n^{SD} + b_n^{BD}(E_0)$, and c_n^{BQ} (*right-hand scale*) obtained from experimental azimuthal anisotropic dependences for FH (*top panel*) and SH (*bottom panel*) intensities from (110) surface. *Lines* are fits to data by the model discussed in the text

harmonic intensity is connected with the nonlinear optical properties of the interface. The total electric field detected by the PMT results from the interference of DC-induced and bias-independent waves of the *n*th harmonic. A large amplitude of the bias-independent harmonic field relative to the DC-dependent harmonic field alters the bias dependence of harmonic intensities from parabolic; the minimum shifts far away from the flat band voltage, or may even disappear. This type of bias dependence of higher harmonic fields is observed in our experiments and shown in Figs. 3 and 7.

Azimuthal angular dependences of DC-induced terms in higher harmonic nonlinear polarizations are presented in Table 3. Although for fixed bias it is not possible to separate bulk quadrupole, surface dipole and DC-induced bulk dipole terms from anisotropic dependences, the bias dependent part of Fourier components allows estimation of the relative value of field-induced and bias-independent terms. Figure 7 shows the experimental bias dependences and fits in the frame of the above electro-physical model of Fourier components $a_n = a_n^{BD} + a_n^{SD} + a_n^{BD}(E_0)$, $b_n = b_n^{BD} + b_n^{SD} + b_n^{BD}(E_0)$ and c_n^{BQ} for SH and FH from the (110) surface. Each Fourier component is the combination of nonlinear susceptibilitiy tensor components with the Fresnel factors at the fundamental and harmonic wavelengths. Therefore, it is not surprising that, for instance for (110) surface, bias-independent and DC-induced parts of a_2 for SH have the same sign, while bias-independent and DC-dependent parts of a_4 for FH have opposite signs. This leads to a different bias dependence of the total a_2 and a_4 (see Fig. 7): a_2 increases while a_4 decreases with increasing bias. Figure 7 shows that the amplitude of FH electromodulation, a_4, is even larger than a_2 for EFISH generation: $\Delta a_4/a_4 = 0.2$, $\Delta a_2/a_2 = 0.1$.

The fractional amplitude of bias modulation of the TH intensity is approximately 0.04. Thus the DC-induced TH field is a only a small fraction of the more intense bulk bias-independent TH field. However, this latter bias-independent contribution serves as an amplifier for the DC-induced contribution because of a cross-term in the TH intensity resulting

Table 3. Azimuthal dependence of the DC-electric-field dependent polarizations at FH, TH and Sh wavelength (for *p*-*p* polarization combination)

	(111)	(110)
FHG	$P_4^{BD}(E_0) = a_4^{BD}(E_0) + b_4^{BD}(E_0)\cos(3\Psi)$	$P_4^{BD}(E_0) = a_4^{BD}(E_0) + b_4^{BD}(E_0)\cos(2\Psi) + c_4^{BD}(E_0)\cos(4\Psi)$
THG	$P_3^{SD}(E_0) = a_3^{SD}(E_0) + b_3^{SD}(E_0)\cos(3\Psi)$	$P_3^{SD}(E_0) = a_3^{SD}(E_0) + b_3^{SD}(E_0)\cos(2\Psi)$
SHG	$P_2^{BD}(E_0) = a_2^{BD}(E_0) + b_2^{BD}(E_0)\cos(3\Psi)$	$P_2^{BD}(E_0) = a_2^{BD} + b_2^{BD}(E_0)\cos(2\Psi)$

from interference of these two TH fields:

$$I(3\omega) = \left(E^{\text{bulk, D}}(3\omega)\right)^2 + \left(E^{\text{surf, D}}(3\omega, E_0)\right)^2 + 2E^{\text{surf, D}}(3\omega, E_0)E^{\text{bulk, D}}(3\omega)\cos(\Delta\Phi)\,, \qquad (11)$$

where $\Delta\Phi$ is the phase difference between bulk and surface (or in other words, DC-induced and bias-independent) TH waves. The stronger the bulk bias-independent TH field, the stronger the cross-term. Thus, even though the second (pure bias-dependent) term in (11) may be almost negligible, DC-modulation becomes observable because of the cross-term. This demonstrates the main advantage of TH generation as a surface probe in comparison with SHG: TH generation is less invasive because it requires weaker fundamental intensity to be detected.

3 Conclusions

In conclusion, third and fourth harmonic generation have been systematically studied at buried Si(111)-SiO_2 and Si(110)-SiO_2 interfaces. A systematic experimental analysis and phenomenological description of azimuthal anisotropy of TH and FH intensities were performed for (111) and (110) surfaces of O_h-symmetric Si single crystals. DC-electric-field induced effects in third and fourth harmonic generation were studied at buried Si(111)-SiO_2 and Si(110)-SiO_2 interfaces in Si-SiO_2-Cr MOS structures. DC-electric-field induced FH generation is observed at both Si(111)-SiO_2 and Si(110)-SiO_2 interfaces whereas DC-electric-field induced TH generation is observed only at Si(111)-SiO_2.

A phenomenological model developed recently for EFISH generation has been extended to TH and FH generation. DC-electric-field induced FH generation is governed in centrosymmetric semiconductors by a bulk dipole fifth-order susceptibility. For silicon probed at 800 nm fundamental wavelength the corresponding nonlinear sources are localized in a subsurface layer 15 nm thick. In contrast to electro-induced FH, DC-electric-field induced TH generation in centrosymmetric semiconductors is governed by *surface* dipole fourth-order susceptibility which is forbidden in the bulk by symmetry considerations. DC-electric-field induced TH generation results from optical interference between bias-dependent surface and bias-independent bulk contributions to the third-order nonlinear polarization. The cross-term in the TH intensity explains both the bias dependence of the TH signal and its surface sensitivity.

Acknowledgements. This work was supported by the U.S. AFOSR DARPA MURI Contract F49620-95-1-0475, the Robert Welch Foundation (Grant F-1038), the Texas Advanced Technology Program (ATPD-178), the U.S. National Science Foundation (NSF) Science and Technology Center Program (Grant CHE-8920120), U.S. NSF Grant PHY-9417558 for U.S.–Russia Cooperative Research, the Russian Foundation for Basic Research (RFBR) grants 97-02-17919, 97-02-17923, RFBR grant 96-15-96420 for the Leading Russian Scientific Schools, Russian Federal Integration Program "Center of Fundamental Optics and Spectroscopy".

References

1. T.F. Heinz: In *Nonlinear Surface Electromagnetic Phenomena*, ed. by H.-E. Ponath, G.I. Stegeman (North Holland, Amsterdam 1991) p. 355
2. J.F. McGilp: Prog. Surf. Sci. **49**, 1 (1995)
3. R.M. Corn, D.A. Higgins: Chem. Rev. **94**, 107 (1994); G.L. Richmond, J.M. Robinson, V.L. Shannon: Prog. Surf. Sci **28**, 1 (1988)
4. N. Bloembergen, Y.R. Shen: Phys. Rev. **141**, 298 (1966)
5. Y.R. Shen: Surf. Sci. **299**/**300**, 551 (1994)
6. Y.-S. Lee, M.H. Anderson, M.C. Downer: Opt. Lett. **22**, 973 (1997); Y.-S. Lee, M.C. Downer: Opt. Lett. **23**, 918 (1998)
7. J.I. Dadap, X.F. Hu, M.H. Anderson, M.C. Downer, J.K. Lowell, O.A. Aktsipetrov: Phys. Rev. B **53**, 7607R (1996)
8. O.A. Aktsipetrov, A.A. Fedyanin, E.D. Mishina, A.N. Rubtsov, C.W. van Hasselt, M.A.C. Devillers, Th. Rasing: Phys. Rev. B **54**, 1825 (1996); P. Godefroy et al.: Appl. Phys. Lett. **68**, 1981 (1996)
9. O.A. Aktsipetrov, E.D. Mishina: Dokl. Akad. Nauk SSSR **274**, 65 (1984) (Sov. Phys. Dokl. **29**, 37 (1984))
10. Z. Xu, X.F. Hu, D. Lim, J.G. Ekerdt, M.C. Downer: J. Vac. Sci. Technol. B **15**, 1059 (1997)
11. P. Bratu, U. Höfer: Phys. Rev. Lett. **74**, 1625 (1995)
12. P.R. Fischer, J.L. Daschbach, G.L. Richmond: Chem. Phys. Lett. **218**, 200 (1994)
13. J.I. Dadap, P.T. Wilson, M.H. Anderson, M.C. Downer, M. ter Beek: Opt. Lett. **22**, 901 (1997)
14. O.A. Aktsipetrov, A.A. Fedyanin, A.V. Melnikov, E.D. Mishina, A.N. Rubtsov, M.H. Anderson, P.T. Wilson, M. ter Beek, X.F. Hu, J.I. Dadap, M.C. Downer: Phys. Rev. B (1998) to be published
15. P. Guyot-Sionnest, Y.R. Shen: Phys. Rev. B **33**, 8254 (1986)